DOI: 10.1002/asia.201301305

Two Organic–Inorganic Hybrid 3D $\{P_5W_{30}\}$-Based Heteropolyoxotungstates with Transition-Metal/Ln–Carboxylate–Ln Connectors

Yan-Ying Li,[a] Jun-Wei Zhao,*[b] Qi Wei,[c] Bai-Feng Yang,[a] Huan He,[a] and Guo-Yu Yang*[a, c]

Abstract: Two unique organic–inorganic hybrid polyoxometalates constructed from Preyssler-type $[Na(H_2O)P_5W_{30}O_{110}]^{14-}$ ($\{P_5W_{30}\}$) subunits and TM/Ln–carboxylate–Ln connectors (TM = transition metal, Ln = lanthanide), $KNa_7[\{Sm_6Mn(\mu\text{-}H_2O)_2(OCH_2COO)_7(H_2O)_{18}\}\{Na(H_2O)P_5W_{30}O_{110}\}]\cdot 22H_2O$ (**1**) and $K_4[\{Sm_4Cu_2(gly)_2(ox)(H_2O)_{24}\}\{NaP_5W_{30}O_{110}\}]Cl_2\cdot 25H_2O$ (**2**; gly = glycine, ox = oxalate) have been hydrothermally synthesized and characterized by elemental analyses, IR spectra, UV/Vis-NIR spectra, thermogravimetric analyses, power X-ray diffraction, and single-crystal X-ray diffraction. Compound **1** displays one interesting 3D framework built by three types of subunits, $\{P_5W_{30}\}$, $[Sm_2Mn(\mu\text{-}H_2O)_2(OCH_2COO)_2(H_2O)_5]^{4+}$, and $[Sm_4(OCH_2COO)_5(H_2O)_{13}]^{2+}$, whereas **2** also manifests the other intriguing 3D architecture created by three types of subunits, $\{P_5W_{30}\}$, $[SmCu(gly)(H_2O)_8]^{4+}$, and $[Sm_2(ox)(H_2O)_8]^{4+}$. To our knowledge, **1** and **2** are the first 3D frameworks that contain $\{P_5W_{30}\}$ units and TM/Ln–carboxylate–Ln connectors. The fluorescent properties of **1** and **2** have been investigated.

Keywords: carboxylic acids · luminescence · organic–inorganic hybrid composites · polyoxometalates · transition metals

Introduction

Nowadays, the featured oxygen-rich surfaces, high charge densities, and controllable sizes of polyoxoanions have made polyoxometalate (POM)-based materials popular and attractive because of their potential applications in catalysis, magnetism, electrochemistry, and photochemistry.[1] Different kinds of polyoxoanions, including Keggin, Wells–Dawson, Lindqvist, and so on, have been utilized as synthons for the constructions of 0, 1, 2, and 3D transition-metal (TM)-substituted or bridging POM-based materials.[2] Lanthanide (Ln) cations are also suitable for linking POM fragments into Ln-containing POMs (LCPs) with novel structures and interesting luminescence, magnetic, and Lewis acid catalytic properties.[3] Since Peacock and Weakly reported $[LnW_{10}O_{35}]^{6/7-}$ in 1971,[4] the functionalization of polyoxoanions by Ln cations has been heavily exploited, directly resulting in the appearance of many LCP aggregates.[5–8] In contrast, much less attention has been paid to hybrid compounds including POMs and TM/Ln heterometallic complexes that act as connectors (HPTLCCs). With the rapid development of POM chemistry, the design and synthesis of HPTLCCs has been a current challenging domain. Since the first family of HPTLCCs, $[Ln(H_2O)_5\{Ni(H_2O)\}_2As_4W_{40}O_{140}]^{21-}$ ($Ln = Y^{III}/Ce^{III}/Pr^{III}/Nd^{III}/Sm^{III}/Eu^{III}/Gd^{III}$), was discovered,[9] such work has been continuously exploited. Some typical research findings are listed here: HPTLCCs based on lacunary Keggin fragments, such as $[\{(VO)_2Dy(H_2O)_4K_2(H_2O)_2Na(H_2O)_2\}(B\text{-}\alpha\text{-}AsW_9O_{33})_2]^{8-}$;[10] 1D $[\{Ln(PW_{11}O_{39})_2\}\{Cu_2(bpy)_2(\mu\text{-}ox)\}]^{9-}$ ($Ln = La^{III}/Pr^{III}/Eu^{III}/Gd^{III}/Yb^{III}$; bpy = 2,2′-bipyridyl, ox = oxalate);[11] sandwich-type, trimeric, hexameric, $\{DyMn^{III}_4\}$ cubane-appended HPTLCCs;[12] 3D porous $[\{Ag_3(H_2O)_2\}\{Ce_2(H_2O)_{12}\}\{H_2W_{11}Ce(H_2O)_4O_{39}\}_2]^{5-}$;[13] $\{Ce_2Mn_2\}$- or $\{CeCu_3\}$-substituted sandwich-type germanotungstates;[14] cubane-$\{LnCu_3(OH)_3O\}$-inserted silico-tungstates ($Ln = Gd^{III}/Eu^{III}$),[15a] and a 1D double-chain $[(\gamma\text{-}SiW_{10}O_{36})_2\{Cr(OH)(H_2O)\}_3\{La(H_2O)_7\}_2]^{4-}$;[15b] pyrazine-2,3-dicarboxylate/oxalate/organoamine-containing HPTLCCs;[16] and 1D oxalate/acetate-bridging HPTLCCs.[17] In addition, other HPTLCCs including monolacunary Keggin units were also summarized:[18] HPTLCCs based on lacunary Dawson fragments such as $[\{\alpha\text{-}P_2W_{15}O_{56}\}_6\{Ce_3Mn_2(\mu_3\text{-}O)_4(\mu_2\text{-}OH)_2\}_3(\mu_2\text{-}OH)_2(H_2O)_2(PO_4)]^{47-}$[19a] and $[\{\alpha\text{-}P_2W_{16}O_{57}(OH)_2\}\{CeMn_6O_9$

[a] Y.-Y. Li, B.-F. Yang, H. He, Prof. G.-Y. Yang
DOE Key Laboratory of Cluster Science, School of Chemistry
Beijing Institute of Technology, Beijing 100081 (China)
Fax: (+86) 10-6891-8572
E-mail: ygy@bit.edu.cn

[b] Dr. J.-W. Zhao
Henan Key Laboratory of Polyoxometalate Chemistry
College of Chemistry and Chemical Engineering
Henan University, Kaifeng, Henan 475004 (China)
Fax: (+86) 371-2388-1589
E-mail: zhaojunwei@henu.edu.cn

[c] Q. Wei, Prof. G.-Y. Yang
State Key Laboratory of Structural Chemistry
Fujian Institute of Research on the Structure of Matter
Chinese Academy of Sciences, Fuzhou, Fujian 350002 (China)
Fax: (+86) 591-8371-0051
E-mail: ygy@fjirsm.ac.cn

Supporting information for this article is available on the WWW under http://dx.doi.org/10.1002/asia.201301305.

$(O_2CCH_3)_8\}]^{2-}$;[19b] two $\{P_2W_{12}\}$-based $[K_3\subset\{GdMn(H_2O)_{10}\}\{HMnGd_2(tart)O_2(H_2O)_{15}\}\{P_6W_{42}O_{151}(H_2O)_7\}]^{11-}$ (tart = tartrate), $[K_3\subset\{GdCo(H_2O)_{11}\}_2\{P_6W_{41}O_{148}(H_2O)_7\}]^{13-}$;[20a] and a cyclic trimeric $\{[Ce_3Mn_2O_6(OAc)_6(H_2O)_9]_2Mn_2P_2W_{16}O_{60}]_3\}^{20-}$ (Ac = acetyl);[20b] and a horseshoe-shaped Fe_{16}-containing $[Fe_{16}O_2(OH)_{23}(H_2O)_9P_8W_{49}O_{189}Ln_4(H_2O)_{19}]^{11-}$ (Ln = Eu^{III}/Gd^{III}).[21]

Of the above-mentioned compounds, most previously reported HPTLCCs are based on small POM (such as Keggin or Dawson) fragments. However, the search for and investigation of HPTLCCs that are constructed from large POM moieties are very rare to date,[21] which not only provides us with a great opportunity, but also a great impetus to explore this domain. The drum-shaped $[Na(H_2O)P_5W_{30}O_{110}]^{14-}$ ($\{P_5W_{30}\}$) polyoxoanion, as the second largest phosphotungstate precursor near to the cyclic $\{P_8W_{48}\}$ precursor, was selected as the candidate by us because 1) it has been little investigated since it was discovered in 1970;[22] 2) it is very stable over a large pH range (pH stability range 0–10) and has its abundant surface oxygen atoms exposed, which offers a strong likelihood to bind TM and Ln cations, thereby constructing novel hybrids including $\{P_5W_{30}\}$ and TM–Ln heterometallic cations if the reaction conditions are appropriate; and 3) it is bulky and has high negative surface charges, which is more favorable to realizing the purpose of point (2). The $\{P_5W_{30}\}$ polyoxoanion consists of a cyclic arrangement of five PW_6O_{22} units, which was first reported by Preyssler,[22] and its structure was resolved through X-ray diffraction by Pope and co-workers 15 years later.[23] Limited studies have proved that $\{P_5W_{30}\}$-based materials show good potential in catalysis, materials science, and organic synthesis.[24] The $\{P_5W_{30}\}$ anion shows excellent electrochromic performance in terms of optical contrast, stability, and reversibility.[25] In 2011, the $\{P_5W_{30}\}$-type POM as a mild and efficient catalyst was applied to protect the carbonyl compounds.[26] In 2012, a family of mononuclear lanthanoid complexes, $[LnP_5W_{30}O_{110}]^{12-}$ (Ln = Tb^{III}/Dy^{III}/Ho^{III}/Er^{III}/Tm^{III}/Yb^{III}), based on the $\{P_5W_{30}\}$ cluster were shown to exhibit single-molecule magnetic (SMM) behavior.[3f] To sum up, the above-mentioned $\{P_5W_{30}\}$-type POMs in the literature are mainly metal-cation-encapsulated Preyssler complexes, whereas Preyssler's metal–organic-complex-modified or -extended structures have rarely been reported (see the Supporting Information).[27] This situation indicates that it is a great challenge to make novel POMs built by this precursor and TM–Ln cations. In this work, flexible acid ligands (glycolic acid or iminodiacetic acid) were chosen as the bridging agent because the small steric size of ligands avoids crowding in the vicinity of the $\{P_5W_{30}\}$ anion and encourages further connectivity.

Herein, we systematically explored the reactions of Sm^{3+}, Mn^{2+}, or Cu^{2+} ions with the Preyssler anion and have successfully obtained two 3D organic–inorganic HPTLCCs $KNa_7[\{Sm_6Mn(\mu\text{-}H_2O)_2(OCH_2COO)_7(H_2O)_{18}\}\{Na(H_2O)\text{-}P_5W_{30}O_{110}\}]\cdot 22H_2O$ (**1**) and $K_4[\{Sm_4Cu_2(gly)_2(ox)(H_2O)_{24}\}\{NaP_5W_{30}O_{110}\}]Cl_2\cdot 25H_2O$ (**2**; gly = glycine). Compound **1** displays one interesting 3D framework built by three types of subunits, $\{P_5W_{30}\}$, $[Sm_2Mn(\mu\text{-}H_2O)_2(OCH_2\text{-}COO)_2(H_2O)_5]^{4+}$, and $[Sm_4(OCH_2COO)_5(H_2O)_{13}]^{2+}$, whereas **2** also manifests another intriguing 3D architecture created by three types of subunits, $\{P_5W_{30}\}$, $[SmCu(gly)(H_2O)_8]^{4+}$, and $[Sm_2(ox)(H_2O)_8]^{4+}$. To the best of our knowledge, **1** represents the highest connection of the Preyssler anion (eleven Sm ions and two Mn ions) to date in the coordination chemistry of Ln elements.[27a,c] Compounds **1** and **2** represent the first 3D HPTLCCs built by $\{P_5W_{30}\}$ subunits and TM/Ln–carboxylate–Ln connectors. Furthermore, the room-temperature solid-state photoluminescence properties of **1** and **2** have been examined.

Abstract in Chinese:
在水热条件下，以 Preyssler 型多金属氧酸盐 $K_{12.5}Na_{1.5}[Na(H_2O)P_5W_{30}O_{110}]\cdot 15H_2O$ 为前躯体得到了 2 个新颖的过渡/稀土金属–羧酸–稀土金属杂核的有机-无机杂化产物，并通过 X-射线单晶衍射，元素分析，红外光谱，紫外光谱，热分析和 X-射线粉末衍射等进行了表征。有趣地是：化合物 **1** 是一例由$\{P_5W_{30}\}$, $[Sm_2Mn(\mu\text{-}H_2O)_2(OCH_2COO)_2(H_2O)_5]^{4+}$ 和 $[Sm_4(CH_2OCOO)_5(H_2O)_{13}]^{2+}$等三种亚单元构建的三维结构；而化合物 **2** 则是由$\{P_5W_{30}\}$, $[SmCu(gly)(H_2O)_8]^{4+}$和 $[Sm_2(ox)(H_2O)_8]^{4+}$等亚单元构建的另一种三维网络。据我们所知，**1** 和 **2** 代表了首例基于$\{P_5W_{30}\}$型簇单元和过渡/稀土金属–羧酸–稀土金属构建的三维结构。同时，本文中还讨论了化合物 **1** 和 **2** 的发光性能。

Results and Discussion

Synthesis

Over the past few years, our group has successfully used the reaction strategy of a combination between the reaction system of lacunary polyoxotungstate (POT) precursors and TM ions and the hydrothermal method to make TM-substituted POTs, thereby resulting in a series of novel high-nuclear TM-substituted POTs (see the Supporting Information).[2e–f,28–33] However, it is a great challenge to make novel POMs built from other precursors and metal-ion clusters.

In recent years, a number of HPTLCCs have been reported that are constructed from lacunary Keggin-type or Dawson-type blocks. To obtain novel HPTLCCs, the $\{P_5W_{30}\}$ precursor with larger size and higher negative charges was a preferred choice. The $\{P_5W_{30}\}$ unit is very stable over a large pH range, which is very advantageous for making HPTLCCs that contain $\{P_5W_{30}\}$ units under hydrothermal conditions. As we know, the system that contains Ln, TM,

POMs, and organic ligands usually leads to immediate precipitation rather than crystallization.[17a,18n] Thus, we chose the NaAc/HAc (Ac = acetyl) buffer solution and the hydrothermal method to exploit this system because the solubility of reactants can be increased, which is beneficial to the improved crystallization and the control of the crystal quality.[18o,30] On the other hand, the utilization of the organic ligand is also crucial for making organic–inorganic HPTLCCs. Flexible ligands should be chosen as the bridging agent because the small steric size of the ligands avoids crowding in the vicinity of the $\{P_5W_{30}\}$ anion and encourages further connectivity. Moreover, Ln cations prefer O to N donors, whereas TM ions have a tendency to coordinate to with both O and N donors. Thus, small ligands with N and O donors such as glycine and H_2IDA (IDA = iminodiacetic acid) were employed to make organic–inorganic HPTLCCs.

Initially, when $K_{12.5}Na_{1.5}[Na(H_2O)P_5W_{30}O_{110}]\cdot 15H_2O$, $Sm(NO_3)_3\cdot 6H_2O$, $Mn(ClO_4)_2\cdot 6H_2O$, and glycine in sodium acetate buffer were mixed at 120 °C for 5 days, no crystal was discovered. When glycolic acid replaced glycine under the same conditions, fortunately, light yellow block crystals of **1** were obtained. Nevertheless, when H_2IDA replaced glycolic acid under the same conditions, only amorphous precipitates were obtained. When $Mn(ClO_4)_2$ was replaced by $CuCl_2\cdot 2H_2O$ under the same conditions as **1**, a purple ball-type crystalline substance appeared, but we could not determine its structure. To investigate different TM cations, when Cr^{III}, Cu^{II}, Co^{II}, Fe^{II}, or Ni^{II} cations replaced the Mn^{II} ion, compound **2** was isolated by reaction of $K_{12.5}Na_{1.5}[Na(H_2O)P_5W_{30}O_{110}]\cdot 15H_2O$, $Sm(NO_3)_3\cdot 6H_2O$, $CuCl_2\cdot 5H_2O$, and H_2IDA in sodium acetate buffer at 120 °C for 5 days, during which IDA^{2-} was transformed into coordinated oxalate and glycine ligands (Scheme 1). When oxalic acid and glycine replaced H_2IDA under the same conditions as **2**, the yellow compound $K[Sm(C_2O_4)_2(H_2O)]\cdot 2H_2O$ was obtained.[33b] This comparison suggests that the slow transformation of H_2IDA to oxalate and glycine ligands plays an important role in the formation of **2**. In addition, in the preparation of **1**, if sodium acetate buffer with pH 3.6 was used, compound **1** could not be isolated and only yellow amorphous powders were obtained. In the preparation of **2**, if sodium acetate buffer with pH 5.5 were utilized, **2** could be formed but the yield was decreased from 35 to 20%. These results indicate that the pH of sodium acetate buffer has a crucial effect on the formation and yield of the outcomes.

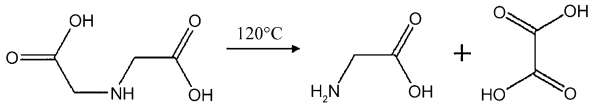

Scheme 1. Schematic view of the decomposition of H_2IDA.

Structural Description

The experimental PXRD patterns of the bulk products of **1** and **2** are in good agreement with the simulated ones from single-crystal X-ray diffraction (see the Supporting Information). The intensity difference between experimental and simulation PXRD patterns is due to the variation in the preferred orientation of the powder sample during collection of the experimental PXRD. The bond-valence sum calculations indicate that all of the W, Mn, Cu, and Sm atoms in **1** and **2** are in the +6, +2, +2, and +3 oxidation states, respectively.[34]

Single-crystal X-ray structural analysis reveals that the structure of **1** contains two noticeable features. First, the drum-shaped Preyssler $\{P_5W_{30}\}$ anion acts as a 13-dentate inorganic ligand that coordinates to 11 Sm ions and 2 Mn ions (Figure 1). Although the Preyssler anion has abundant oxygen atoms available to coordinate to metal ions, its coordination numbers reported are no more than nine. In 2012, $[\{Pr_4(H_2O)_{12}(pydc)_4\}\{Na(H_2O)P_5W_{30}O_{110}\}]^{10-}$ (pydc = pyridine-2,6-dicarboxylic acid) was isolated by Zhang and coworkers in which there are eight Pr^{III} atoms grafted onto a Preyssler anion by means of eight terminal oxygen atoms. Therefore, the 13-coordinate Preyssler anion reported here represents the highest coordinated polyanion to date. Second, **1** contains three distinct building units, one Preyssler subunit, one Mn–Sm heterometallic $[Sm_2Mn(\mu\text{-}H_2O)_2(OCH_2COO)_2(H_2O)_5]^{4+}$ subunit (Figure 2a) and one $[Sm_4(OCH_2COO)_5(H_2O)_{13}]^{2+}$ subunit (Figure 3a), which represents the first 3D framework to consist of $\{P_5W_{30}\}$ subunits and TM/Ln–carboxylic acid–Ln connectors.

The Mn–Sm heterometallic $[Sm_2Mn(\mu\text{-}H_2O)_2(OCH_2COO)_2(H_2O)_5]^{4+}$ subunit is made up of two Sm^{III} (Sm1 and Sm2) ions and one Mn^{II} (Mn1) ion bridged by two $\mu\text{-}H_2O$ molecules and two glycolate ligands (Sm1···Sm2: 6.181 Å, Sm1···Mn1: 4.683 Å, and Sm2···Mn1: 6.678 Å). Two crystallographically independent Sm^{III} ions are nine-coordi-

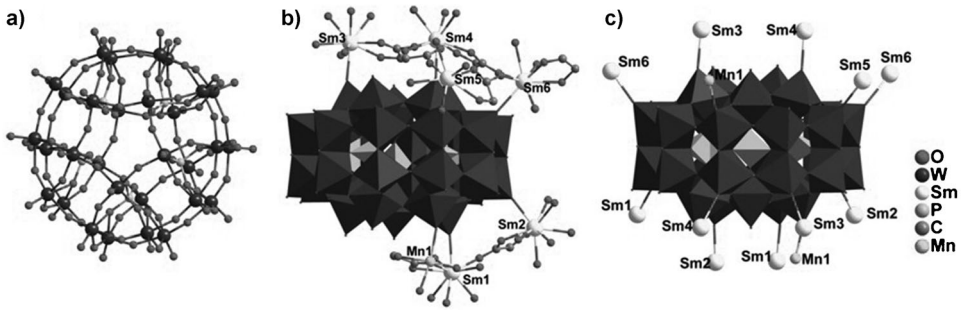

Figure 1. a) Polyhedron representation of the $\{P_5W_{30}\}$ anion. b) Combined polyhedral and ball/stick representation of the molecular structure unit of **1**. All of the hydrogen atoms and water molecules have been omitted for clarity. c) Coordination view of the $\{P_5W_{30}\}$ cluster. Atoms with "A or B" in their labels are symmetrically generated. A: $1-x$, $0.5+y$, $0.5-z$; B: $-0.5+x$, $2.5-y$, $-z$; C: $-1+x$, y, z; D: $-1.5+x$, $2.5-y$, $-z$; E: $-x$, $0.5+y$, $0.5-z$; F: $0.5+x$, $2.5-y$, z; G: $0.5-x$, $2-y$, $-0.5+z$).

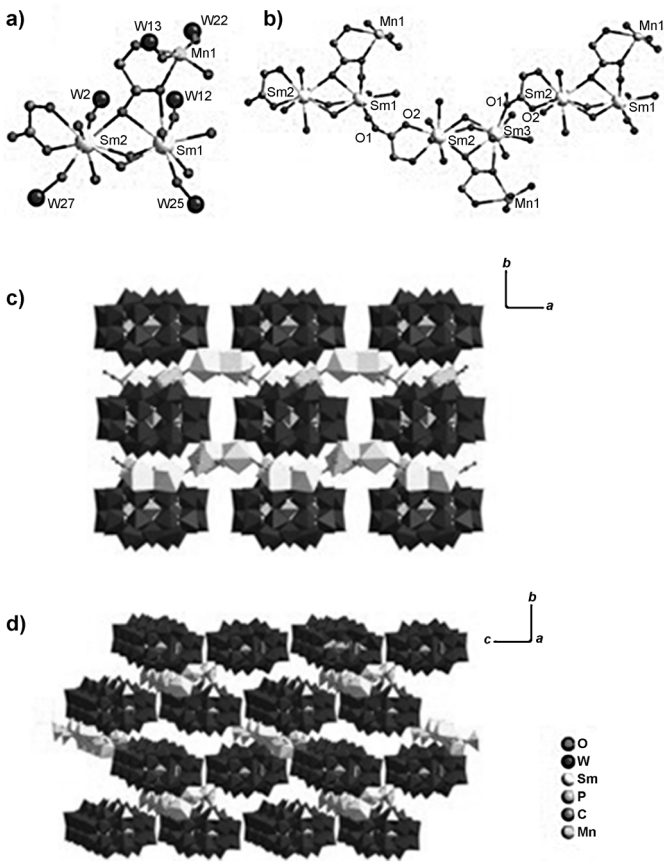

Figure 2. a) The coordination environments of Sm1, Sm2, and Mn1 ions. b) The combination of adjacent $[Sm_2Mn(\mu\text{-}H_2O)_2(OCH_2COO)_2(H_2O)_5]^{4+}$ subunits. c) The 2D architecture built by $\{P_5W_{30}\}$ clusters through $[Sm_2Mn(\mu\text{-}H_2O)_2(OCH_2COO)_2(H_2O)_5]^{4+}$ subunits. d) The 3D infinite extended framework linked by $[Sm_2Mn(\mu\text{-}H_2O)_2(OCH_2COO)_2(H_2O)_5]^{4+}$ subunits.

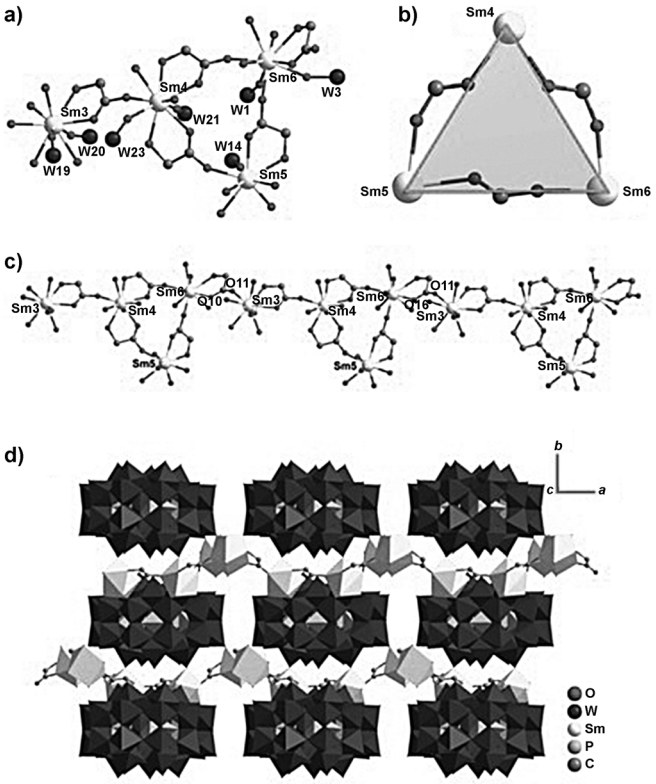

Figure 3. a) The coordination environments of Sm3, Sm4, Sm5, and Sm6 ions. b) View of the $\{Sm_3\}$ metallacycle. c) The chain formed by adjacent $[Sm_4(OCH_2COO)_5(H_2O)_{13}]^{2+}$ subunits. d) The 2D sheet bridged by $[Sm_4(OCH_2COO)_5(H_2O)_{13}]^{2+}$ subunits.

nate and respectively display a monocapped square antiprism for the Sm1 ion [Sm1–O: 2.361(19)–2.695(19) Å] and a tricapped trigonal prism [Sm2–O: 2.396(18)–2.616(19) Å] (see the Supporting Information). The Mn1 ion exhibits the distorted square pyramidal geometry [Mn1–O: 1.78(4)–2.34(3) Å]. The coordination sphere of the Sm1 ion is defined by three aqua ligands, two carboxyl oxygen atoms from one glycolate ligand, and two μ-H_2O molecules, as well as two oxygen atoms from two Preyssler anions. Relative to the Sm1 ion, the Sm2 ion has different coordination environment, which bonds to two μ-H_2O ligands, one hydroxyl oxygen atom, and two carboxyl oxygen atoms from two glycolate ligands, two aqua ligands, and two oxygen atoms from two $\{P_5W_{30}\}$ anions. The coordination sphere of the Mn1 ion is defined by one carboxyl oxygen atom and one hydroxyl atom from one glycolate ligand, one aqua ligand, and two oxygen atoms from two $\{P_5W_{30}\}$ anions. Furthermore, adjacent $\{Sm_2Mn\}$ subunits can be linked by the carboxyl oxygen atoms (O1,O2) (Figure 2b). As illustrated in the Supporting Information, each $\{P_5W_{30}\}$ wheel is covalently bonded to four $[Sm_2Mn(\mu\text{-}H_2O)_2(OCH_2COO)_2(H_2O)_5]^{4+}$ subunits, and each $[Sm_2Mn(\mu\text{-}H_2O)_2(OCH_2COO)_2(H_2O)_5]^{4+}$ subunit is connected with four $\{P_5W_{30}\}$ wheels, thus resulting in the 2D architecture (Figure 2c). And then neighboring 2D sheets are interconnected by means of $\{Sm_2Mn\}$ subunits, thereby giving rise to a 3D infinite extended framework (Figure 2d).

There are four crystallographically unique Sm^{III} ions in $[Sm_4(OCH_2COO)_5(H_2O)_{13}]^{2+}$. The Sm3 and Sm4 ions adopt a nine-coordinate tricapped trigonal prismatic geometry, and the Sm5 ion adopts an eight-coordinate dodecahedral geometry, whereas the Sm6 ion adopts a nine-coordinate monocapped square antiprismatic geometry [Sm3–O: 2.36(2)–2.53(2) Å, Sm4–O: 2.32(2)–2.56(2) Å, Sm5–O: 2.324(19)–2.66(4) Å, Sm6–O: 2.29(2)–2.61(2) Å] (see the Supporting Information). The Sm3 ion links four aqua ligands, two carboxyl oxygen atoms, and one hydroxyl from two glycolate ligands, and two oxygen atoms from two Preyssler anions. The Sm4 ion bonds two aqua ligands, three carboxyl oxygen atoms, and two hydroxyl groups from three glycolate ligands, and two oxygen atoms from two $\{P_5W_{30}\}$ anions. The Sm5 ion is coordinated by four aqua ligands, one hydroxyl, and two carboxyl oxygen atoms from two glycolate ligands, and one oxygen atom from a Preyssler anion. The Sm6 ion joins three aqua ligands, three carboxyl oxygen atoms, and one hydroxyl from three glycolate ligands, and two oxygen atoms from two Preyssler anions. Furthermore, Sm3 and Sm4 ions can be linked by the carboxyl group from a glycolate ligand, and the distance of Sm3···Sm4 is 6.603 Å. Sm4,

Sm5, and Sm6 ions are bridged by three carboxyl groups from three glycolate ligands to form a $\{Sm_3\}$ metallocycle (Figure 3b) that can be viewed as an approximate isosceles triangle [Sm4···Sm5: 6.548 Å, Sm5···Sm6: 6.753 Å, Sm4···Sm6: 6.494 Å]. Adjacent $[Sm_4(OCH_2COO)_5(H_2O)_{13}]^{2+}$ subunits can be linked together by the carboxyl oxygen atoms (Figure 3c). Each Preyssler anion is grafted by three $[Sm_4(OCH_2COO)_5(H_2O)_{13}]^{2+}$ subunits, and each $[Sm_4(OCH_2COO)_5(H_2O)_{13}]^{2+}$ subunit is connected with three $\{P_5W_{30}\}$ wheels, further yielding a 2D sheet (Figure 3d). Finally, each layer can be bridged by $[Sm_2Mn(\mu\text{-}H_2O)_2(OCH_2COO)_2(H_2O)_5]^{4+}$ linkers to give rise to a 3D framework (Figure 4).

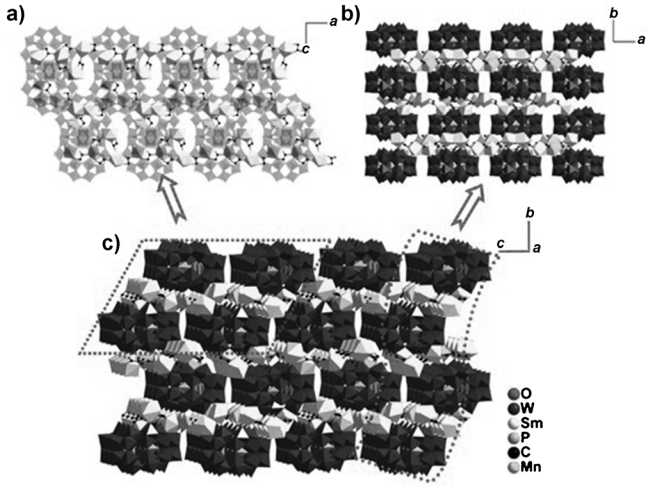

Figure 4. a) Polyhedral view of the 2D sheet of **1** along the *a* axis. b) Polyhedral view of the 2D sheet of **1** along the *c* axis. c) The 3D framework of **1**.

When $CuCl_2{\cdot}5H_2O$ and H_2IDA replaced $Mn(ClO_4)_2{\cdot}6H_2O$ and glycolic acid, respectively, under the same conditions, compound **2** was obtained, which possesses an entirely different structure from **1**. Single-crystal X-ray structural analysis reveals that the asymmetric unit of **2** contains one-half Preyssler anion, one gly-coordinated $[SmCu(gly)(H_2O)_8]^{4+}$ unit, one-half ox-coordinated $[Sm_2(ox)(H_2O)_8]^{4+}$ unit, and two potassium cations (Figure 5a). In the structure of **2**, the $\{P_5W_{30}\}$ anion acts as a ten-dentate inorganic ligand that coordinates to 10 Sm^{3+} centers (Figure 5b). Two Sm^{III} ions (Sm1 and Sm2) are crystallographically independent. The Sm1 ion is nine-coordinate with the average Sm1−O distances of 2.46 Å and displays a distorted monocapped square antiprismatic environment defined by five aqua ligands, three oxygen atoms from three Preyssler anions, as well as one carboxyl oxygen atom from one μ_3-gly ligand (see the Supporting Information). It is noteworthy that the μ_3-gly also chelates to the Cu1 ion through the carboxylate and amino groups [Cu1−O1: 2.04(3) Å, Cu1−N1: 2.267(18) Å] that form the TM–Ln $[SmCu(gly)(H_2O)_8]^{4+}$ subunit [Sm1···Cu1: 6.258 Å]. The square-pyramidal Cu1 ion is completed by other oxygen atoms from three aqua ligands [Cu1−O: 2.08(4)–2.652 Å] (Figure 5c).

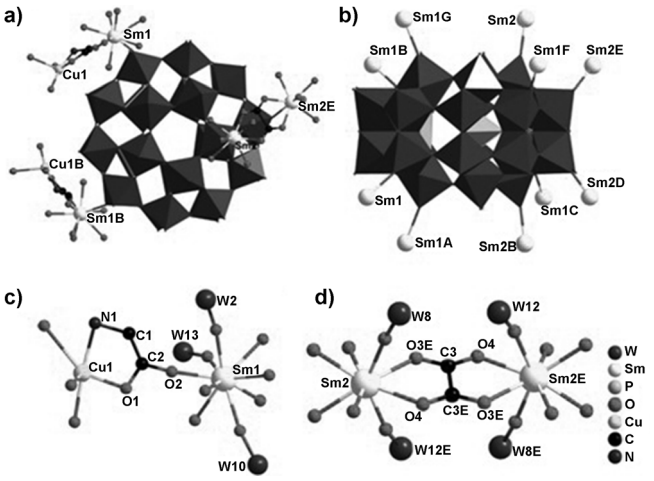

Figure 5. a) The molecular structure unit of **2**. b) Coordination view of the $\{P_5W_{30}\}$ cluster. c) Coordination environment of Sm1 and Cu1 ions. d) Coordination environment of the Sm2 ions. Atoms with "A or B" in their labels are symmetrically generated. A: $2-x$, $1-y$, $1-z$; B: $2-x$, y, $0.5-z$; C: $0.5+x$, $0.5+y$, z; D: x, $2-y$, $0.5+z$; E: $2-x$, $2-y$, $-z$; F: $1.5-x$, $0.5+y$, $0.5-z$; G: x, $1-y$, $-0.5+z$.

As far as a Preyssler anion is concerned, there are six $[SmCu(gly)(H_2O)_8]^{4+}$ subunits in total grafted onto it through six Sm-O-W linkers (Figure 6a), whereas each $[SmCu(gly)(H_2O)_8]^{4+}$ subunit is connected with three Preyssler anions, thus resulting in a 3D framework (Figure 6b). The $[Sm_2(ox)(H_2O)_8]^{4+}$ subunit of **2** is made up of two Sm2 ions bridged by an oxalate in the usual bisbidentate fashion with the Sm···Sm distance of 6.306 Å (Figure 5d). The Sm2 ion adopts an eight-coordinate dodecahedral coordination geometry that is ligated by four aqua ligands, two carboxyl oxygen atoms from one oxalate ligand, and two oxygen atoms from two Preyssler anions [Sm2−O: 2.321(19)-2.430(17) Å]. As shown in Figure 6c, each Preyssler anion bonds to two $[Sm_2(ox)(H_2O)_8]^{4+}$ subunits as a tetradentate ligand through four oxygen atoms of the Preyssler anions, and $[Sm_2(ox)(H_2O)_8]^{4+}$ subunits bridge adjacent $\{P_5W_{30}\}$ ions to form a 1D zigzag chain along the *c* axis (Figure 6d).

Finally, the $\{P_5W_{30}\}$ anions are extended to a novel 3D network by the $[SmCu(gly)(H_2O)_8]^{4+}$ and $[Sm_2(ox)(H_2O)_8]^{4+}$ subunits (Figure 7a, b). From the topological point of view, $\{P_5W_{30}\}$ anions are a ten-connected node, Sm1 ions are 3-connected nodes, and Sm2 ions are 2-connected nodes, and thus the 3D topological network can be generated with the vertex symbol of $(4^2{\cdot}6)_2(4^6{\cdot}6^{18}{\cdot}8^{21})(4)_2$ (Figure 7c).

IR and UV/Vis-NIR Spectra

IR spectra of **1** and **2** were recorded between 4000 and 400 cm^{-1} with KBr pellets (see the Supporting Information). In both IR spectra, characteristic vibration patterns of the $\{P_5W_{30}\}$ anions, namely, $\nu(P-O_a)$, $\nu(W-O_d)$, and $\nu(W-O_{b/c})$, appear at 1165 and 1081, 935 and 912, and 781 and 753 cm^{-1}

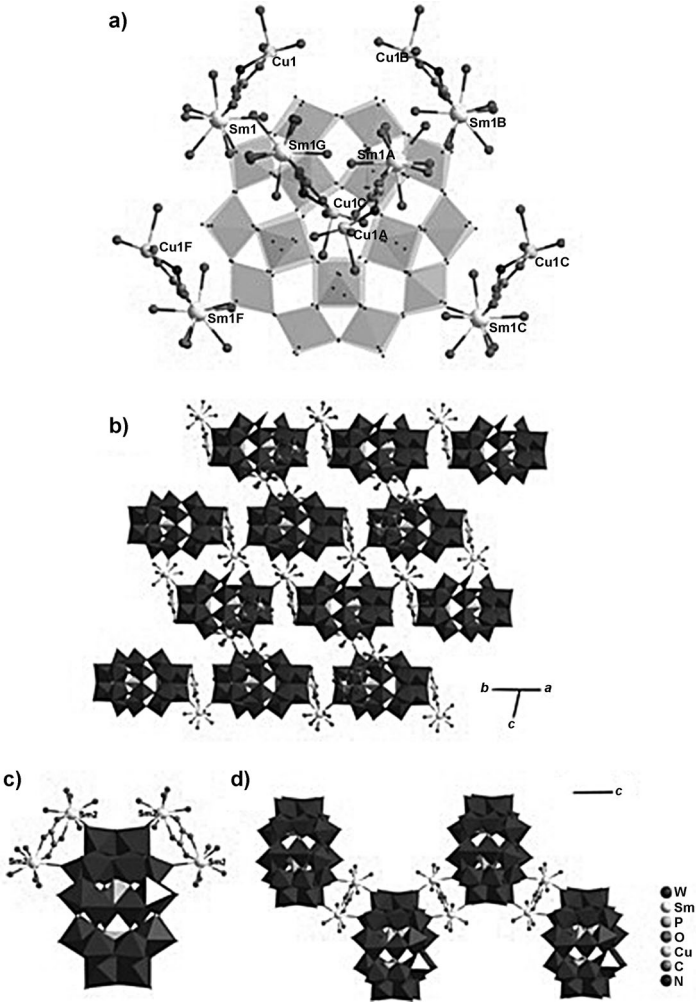

Figure 6. a) A Preyssler anion in connection with six $[SmCu(gly)(H_2O)_8]^{4+}$ subunits. b) The 3D network created by Preyssler anions and $[SmCu(gly)(H_2O)_8]^{4+}$ subunits. c) A Preyssler anion in connection with two $[Sm_2(ox)(H_2O)_8]^{4+}$ subunits. d) The 1D chain constructed from Preyssler anions by $[Sm_2(ox)(H_2O)_8]^{4+}$ bridges along the *c* axis.

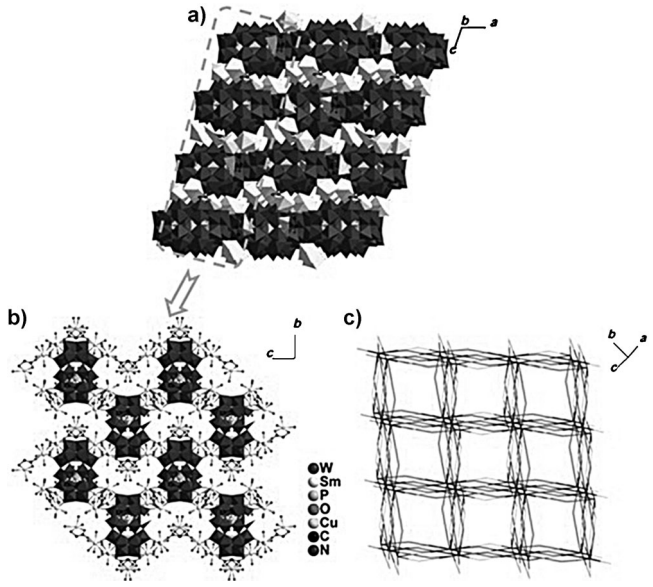

Figure 7. a, b) Polyhedron view of the 2D sheet and the 3D framework of **2**. c) The topological 3D network.

for **1**; and at 1162 and 1082, 935 and 915, and 781 and 741 cm^{-1} for **2**, respectively. Small shifts or splitting in characteristic peaks of $\{P_5W_{30}\}$ might be caused by the coordination of TM or Ln cations. In general, in the IR spectra of **1** and **2**, the carboxylic groups are expected to give rather intense bands from asymmetric (1577–1619 cm^{-1}) and symmetric (1364–1466 cm^{-1}) stretching vibrations. In addition, the bending vibration band of $-CH_2$ group falls at 1448 cm^{-1} for **1** and 1460 cm^{-1} for **2**. Apart from that, a series of peaks appear at 3412–3484 and 2920–2960 cm^{-1} for **1**, or 3400–3500 and 2915–2960 cm^{-1} for **2** may be assigned to the stretching of the O–H and C–H bonds. In summary, the results of the IR spectra are consistent with the single-crystal structural analyses.

The solid-state UV/Vis-NIR spectra of **1** and **2** have been performed at 1800–200 nm at room temperature (Figure 8). The UV spectra of **1** and **2** in the range of 200–340 nm all reveal strong absorption bands centered at 256 and 278 nm,

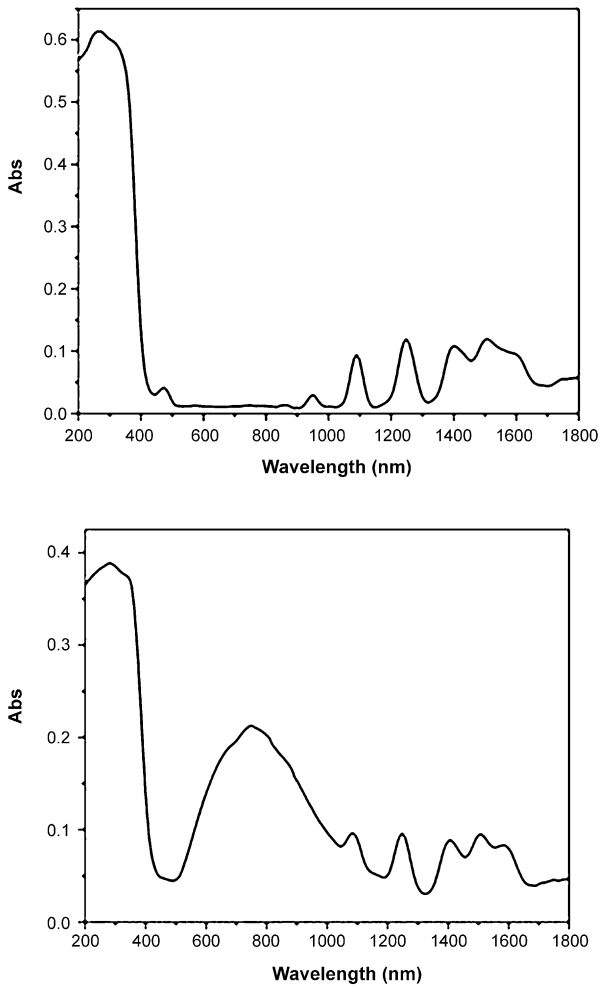

Figure 8. The solid-state UV/Vis-NIR spectra of **1** (top) and **2** (bottom) in the 1800–200 nm range at room temperature.

which are assigned to the pπ–dπ charge-transfer transitions of the $O_{b(c)}\rightarrow W$ bonds.[2e,35] Six absorption bands centered at 948, 1088, 1251, 1404, 1515, and 1583 nm for **1** can be ascribed to the transitions of $^6H_{5/2}\rightarrow{}^6F_{11/2}$, $^6H_{5/2}\rightarrow{}^6F_{9/2}$, $^6H_{5/2}\rightarrow{}^6F_{7/2}$, $^6H_{5/2}\rightarrow{}^6F_{5/2}$, $^6H_{5/2}\rightarrow{}^6F_{3/2}$, and $^6H_{5/2}\rightarrow{}^6F_{1/2}$ of the Sm^{III} cation,[36] respectively. For **2**, visible-NIR spectra exhibit the absorption bands attributable to the d–d transitions of the Cu^{II} ion and the f–f transitions of the Sm^{III} cation. The absorption band at 751 nm attributed to the d–d transitions of the Cu^{II} ion and the absorption bands at 1082, 1248, 1410, 1509, and 1583 nm can be ascribed to the transitions of $^6H_{5/2}\rightarrow{}^6F_{9/2}$, $^6H_{5/2}\rightarrow{}^6F_{7/2}$, $^6H_{5/2}\rightarrow{}^6F_{5/2}$, $^6H_{5/2}\rightarrow{}^6F_{3/2}$, and $^6H_{5/2}\rightarrow{}^6F_{1/2}$ of the Sm^{III} ions, respectively. The absorption band assigned to the $^6H_{5/2}\rightarrow{}^6F_{11/2}$ transitions is overlapped by the strong d–d transitions of the Cu^{II} ion.

Photoluminescence Properties

It is well known that Ln-based complexes can play a prominent role in photoluminescent properties and technological applications in areas such as lasers, light-emitting diodes, cathode rays, plasma displays, optical fibers, optical amplifiers, NIR-emitting materials, and sensory probes,[37] which is related to the electronic properties of the Ln ions: the shielding of the 4f electrons by the outer 5s and 5p electrons results in well-defined absorption and emission bands.[38] Consequently, Ln ions retain their atomic properties in the formation of the complexes. Thus, the solid-state photoluminescence properties of **1** and **2** were investigated at room temperature (Figure 9). When **1** is excited at 410 nm, characteristic luminescent bands of the Sm^{III} ion appear, which are attributed to $^4G_{5/2}\rightarrow{}^6H_{5/2}$ (zero–zero band) at 561 nm, $^4G_{5/2}\rightarrow{}^6H_{7/2}$ (magnetic dipole transition) at 595 nm, and $^4G_{5/2}\rightarrow{}^6H_{9/2}$ (electronic dipole transition) at 641 nm, respectively. The most intense peak in the transition is $^4G_{5/2}\rightarrow{}^6H_{7/2}$ at 595 nm, which is in agreement with other previously reported Sm^{III}-containing compounds.[16c] Relative to **1**, compound **2** does not exhibit excellent photoluminescence under excitation at 400 nm, which displays only one peak in the emission spectrum at 597 nm that is attributed to $^4G_{5/2}\rightarrow{}^6H_{7/2}$. This might be due to the quenching induced by Cu ions,[39] or the lowest triplet-state energy level of the ligand does not match well to the resonance level of the Sm^{3+} ions according to the literature.[40] To determine the fluorescence signals that originate from the POM ligand-to-metal charge-transfer (LMCT) bands or the f–f transitions of the Sm^{III} cations, the photochemistry of the $\{P_5W_{30}\}$ cluster has also been measured at room temperature (see the Supporting Information). The free $\{P_5W_{30}\}$ precursor exhibits fluorescent emission bands at 458, 484, and 528 nm ($\lambda_{ex}=344$ nm). The emission spectra of **1** and **2** display three emission bands at 457, 484, and 527 nm for **1** and at 455, 486, and 529 nm for **2** upon excitation at 344 nm, respectively. Clearly, the emission bands of **1** and **2** are similar to those found for the free precursor in position and shape. Therefore, these emission bands of **1** and **2** can be assigned to $^3T_{1u}\rightarrow{}^1A_{1g}$ transitions that derive from the O→W LMCT transitions, which is in accordance with the work published by Yamase et al. that has shown that the intramolecular energy transfer from the O→W excited states to excited energy levels of the Ln ion can occur in the POM system.[41]

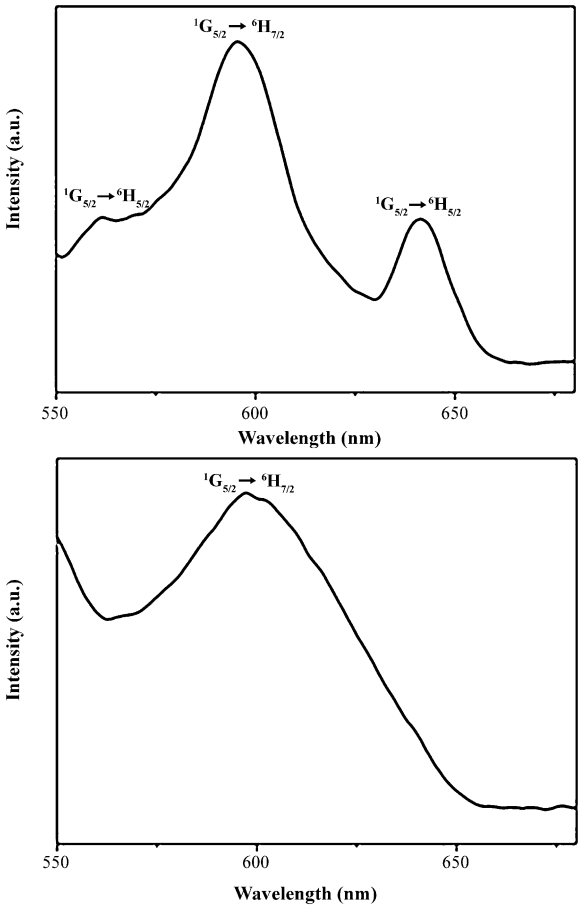

Figure 9. The emission spectra of **1** (top) and **2** (bottom) at room temperature. The emission spectra were recorded at $\lambda_{ex}=410$ nm for **1** and $\lambda_{ex}=400$ nm for **2**.

Thermogravimetric (TG) Analysis

To examine the number of lattice water molecules and the thermal stabilities of **1** and **2**, TG analyses were carried out. Both compounds show a continuous two-step weight loss (see the Supporting Information). The observed total weight loss is 13.58% (calcd 13.06%) for **1** and 12.41% (calcd 11.74%) for **2**. The first weight loss of 4.70% occurs between 30 and 160°C for **1**, which can be assigned to the release of 22 lattice water molecules. However, the first weight loss of 4.92% occurs between 30 and 180°C for **2** that can be assigned to the release of 25 lattice water molecules. Another weight loss of 8.88% for **1** and 7.49% for **2** corresponds to the removal of the organic ligands as well as coordination water molecules.

Conclusion

In summary, two novel HPTLCCs **1** and **2** constructed from $\{P_5W_{30}\}$ clusters, Ln complexes, and TM–Ln complexes, have been successfully synthesized. Compound **1** displays one interesting 3D framework built by three types of subunits, $\{P_5W_{30}\}$, $\{Sm_2Mn(\mu\text{-}H_2O)_2(OCH_2COO)_2(H_2O)_5\}$, and $\{Sm_4(OCH_2COO)_5(H_2O)_{13}\}$, whereas **2** manifests another intriguing 3D architecture created by three types of subunits, $\{P_5W_{30}\}$, $\{SmCu(gly)(H_2O)_8\}$, and $\{Sm_2(ox)(H_2O)_8\}$. To our knowledge, compounds **1** and **2** represent the first $\{P_5W_{30}\}$-based HPTLCCs. Moreover, **1** displays the highest connection of the Preyssler anion (eleven Sm ions and two Mn ions) to date in POM chemistry. Further work is in progress to produce new functional POMs with other circular multilacunary $\{P_8W_{48}\}$ precursors and POMs based on linkages of $\{P_5W_{30}\}$/$\{P_8W_{48}\}$ units and large TM–Ln clusters formed in situ under hydrothermal conditions.

Table 1. Crystallographic data and structural refinements for **1** and **2**.

Compound	**1**	**2**
empirical formula	$C_{14}H_{100}KMnNa_8O_{174}P_5Sm_6W_{30}$	$C_6H_{104}Cl_2Cu_2K_4N_2NaO_{167}P_5Sm_4W_{30}$
M_r	9903.02	9526.03
T [K]	293(2)	293(2)
λ [Å]	0.71073	0.71073
crystal system	orthorhombic	monoclinic
space group	$P2_12_12_1$	$C2/c$
a [Å]	17.8550(4)	29.0354(9)
b [Å]	23.8756(5)	22.1378(6)
c [Å]	34.8405(8)	24.5583(8)
β [°]	90.00	108.987(3)
V [Å^3]	14852.5(6)	14926.7(8)
Z	4	4
D_{calcd} [g cm^{-3}]	4.429	4.239
μ [mm^{-1}]	25.782	25.171
F(000)	16584	16848
data/parameters	30697/2017	16724/933
GOF on F^2	0.831	1.034
final R indices ($I>2\sigma(I)$)	0.0588 (0.0869)	0.0609 (0.1371)
R indices (all data)	0.1169 (0.1052)	0.1170 (0.1562)

Experimental Section

General Methods and Materials

$K_{12.5}Na_{1.5}[Na(H_2O)P_5W_{30}O_{110}]\cdot 15H_2O$ was synthesized according to the literature.[42] All the reagents were purchased commercially and used without further purification. Elemental analyses (C, H, N) were performed with a EuroEA 3000 CHNS/O analyzer. Inductively coupled plasma (ICP) analyses of Na, K, Sm, Mn, Cu, P, and W were conducted with an Ultima 2 spectrometer. IR spectra were recorded with a Smart Omni-Transmission spectrometer over a range of 400–4000 cm^{-1}. Powder XRD patterns were obtained with a Bruker D8 Advance XRD diffractometer with $Cu_{K\alpha}$ radiation ($\lambda=1.54056$ Å). TG analyses were performed with a Mettler Toledo TGA/DSC 1100 analyzer under an air atmosphere with a heating rate of 10 °C min^{-1}. UV/Vis-NIR spectra were obtained with a Shimadzu UV-3600 UV/Vis-NIR spectrometer. Photoluminescence measurements were performed with a Perkin Elmer LS55 fluorescence spectrophotometer.

*Synthesis of $KNa_7[\{Sm_6Mn(\mu\text{-}H_2O)_2(OCH_2COO)_7(H_2O)_{18}\}\{Na(H_2O)P_5W_{30}O_{110}\}]\cdot 22H_2O$ (**1**)*

A mixture of $K_{12.5}Na_{1.5}[Na(H_2O)P_5W_{30}O_{110}]\cdot 15H_2O$ (0.207 g, 0.026 mmol), $Sm(NO_3)_3\cdot 6H_2O$ (0.062 g, 0.14 mmol), $Mn(ClO_4)_2\cdot 6H_2O$ (0.300 g, 0.83 mmol), and glycolic acid (0.100 g, 1.3 mmol) in sodium acetate buffer (8 mL, 0.5 M, pH 5.5) was stirred for 30 min. The resulting mixture was sealed in a 35 mL stainless-steel reactor with a Teflon liner and heated at 120 °C for 5 d, then cooled to room temperature. Light yellow block crystals of **1** were obtained. Yield: 38% based on $K_{12.5}Na_{1.5}[Na(H_2O)P_5W_{30}O_{110}]\cdot 15H_2O$. IR (solid KBr pellets): $\tilde{\nu}=3480$ (w), 1619 (s), 1364 (w), 1165 (s), 1081 (w), 935 (s), 912 (s), 781 (s), 753 cm^{-1} (s); elemental analysis calcd (%) for **1**: C 1.70, H 1.02, Na 1.86, K 0.40, Mn 0.55, Sm 9.14, P 1.57, W 55.70; found: C 2.03, H 1.10, Na 1.55, K 0.12, Mn 0.21, Sm 8.67, P 1.31, W 55.23.

*Synthesis of $K_4[\{Sm_4Cu_2(gly)_2(ox)(H_2O)_{24}\}\{NaP_5W_{30}O_{110}\}]Cl_2\cdot 25H_2O$ (**2**)*

A mixture of $K_{12.5}Na_{1.5}[Na(H_2O)P_5W_{30}O_{110}]\cdot 15H_2O$ (0.300 g, 0.037 mmol), $Sm(NO_3)_3\cdot 6H_2O$ (0.070 g, 0.16 mmol), $CuCl_2\cdot 5H_2O$ (0.200 g, 0.88 mmol), and iminodiacetic acid (0.077 g, 0.58 mmol) in sodium acetate buffer (8 mL, 0.5 M, pH 3.6) was stirred for 10 min. The resulting mixture was sealed in a 35 mL stainless-steel reactor with a Teflon liner and heated at 120 °C for 5 d, then cooled to room temperature. Blue block crystals of **2** were obtained. The glycine ligand and oxalate ligand in the product were from the decomposition of iminodiacetic acid. Yield: 35% based on $K_{12.5}Na_{1.5}[Na(H_2O)P_5W_{30}O_{110}]\cdot 15H_2O$. IR (solid KBr pellets): $\tilde{\nu}=3412$ (w), 1577 (s), 1466 (w), 1162 (s), 1082 (w), 935 (s), 915 (s), 781 (s), 741 cm^{-1} (s); elemental analyses calcd (%) for **2**: C 0.76, H 1.12, N 0.29, Na 0.24, K 1.64, Cu 1.33, Sm 6.31, P 1.63, W 57.89; found: C 1.08, H 1.14, N 0.51, Na 0.10, K 1.23, Cu 1.04, Sm 6.00, P 1.31, W 57.36.

X-ray Crystallography

A suitable single crystal of as-synthesized **1** and **2** was carefully selected under an optical microscope and glued to thin glass fiber with epoxy resin. Intensity data for **1** and **2** were collected with a Gemini A Ultra diffractometer with $Mo_{K\alpha}$ monochromated radiation ($\lambda=0.71073$ Å) in the ω scanning mode at room temperature. The structures were solved by direct methods and refined on F^2 by full-matrix least-squares methods with the SHELX97 program package.[43] In two compounds, only partial lattice water molecules can be accurately assigned from the residual electron peaks, whereas the rest were directly included in the molecular formula based on the elemental analyses and TG analyses. A summary of the crystallographic data and structural determination for **1** and **2** is provided in Table 1.

CCDC-946738 (**1**) and 946737 (**2**) contain the supplementary crystallographic data for this paper. These data can be obtained free of charge from The Cambridge Crystallographic Data Centre via www.ccdc.cam.ac.uk/data_request/cif.

Acknowledgements

This work was supported by the NNSF of China (nos. 91122028, 21221001, 50872133, and 21101055), the NNSF for Distinguished Young Scholars of China (no. 20725101), and the 973 Program (nos. 2014CB932101 and 2011CB932504).

[1] a) B. S. Bassil, M. Ibrahim, R. Al-Oweini, M. Asano, Z. X. Wang, J. van Tol, N. S. Dalal, K. Y. Choi, R. N. Biboum, B. Keita, L. Nadjo, U. Kortz, *Angew. Chem.* **2011**, *123*, 6083–6087; *Angew. Chem. Int. Ed.* **2011**, *50*, 5961–5964; b) S. S. Mal, U. Kortz, *Angew. Chem.* **2005**, *117*, 3843–3846; *Angew. Chem. Int. Ed.* **2005**, *44*, 3777–3780; c) C. Ritchie, A. Ferguson, H. Nojiri, H. N. Miras, Y. F. Song, D. L. Long,

E. Burkholder, M. Murrie, P. Kögerler, E. K. Brechin, L. Cronin, *Angew. Chem.* **2008**, *120*, 5691–5694; *Angew. Chem. Int. Ed.* **2008**, *47*, 5609–5612; d) M. Sadakane, E. Steckhan, *Chem. Rev.* **1998**, *98*, 219–238; e) R. Pardo, M. Zayat, D. Levy, *Chem. Soc. Rev.* **2011**, *40*, 672–687; f) S. G. Mitchell, C. Streb, H. N. Miras, T. Boyd, D. L. Long, L. Cronin, *Nat. Chem.* **2010**, *2*, 308–312.

[2] a) F. Hussain, B. S. Bassil, L.-H. Bi, M. Reicke, U. Kortz, *Angew. Chem.* **2004**, *116*, 3567–3571; *Angew. Chem. Int. Ed.* **2004**, *43*, 3485–3488; b) Z. Zhang, Y. Qi, C. Qin, Y. Li, E. Wang, X. Wang, Z. Su, L. Xu, *Inorg. Chem.* **2007**, *46*, 8162–8169; c) X. Fang, P. Kögerler, Y. Furukawa, M. Speldrich, M. Luban, *Angew. Chem.* **2011**, *123*, 5318–5322; *Angew. Chem. Int. Ed.* **2011**, *50*, 5212–5216; d) X. L. Wang, C. Qin, E. B. Wang, Z. M. Su, Y. G. Li, L. Xu, *Angew. Chem.* **2006**, *118*, 7571–7574; *Angew. Chem. Int. Ed.* **2006**, *45*, 7411–7414; e) S. T. Zheng, J. Zhang, J. M. Clemente-Juan, D. Q. Yuan, G. Y. Yang, *Angew. Chem.* **2009**, *121*, 7312–7315; *Angew. Chem. Int. Ed.* **2009**, *48*, 7176–7179; f) S. T. Zheng, J. Zhang, G. Y. Yang, *Angew. Chem.* **2008**, *120*, 3973–3977; *Angew. Chem. Int. Ed.* **2008**, *47*, 3909–3913; g) S. T. Zheng, J. Zhang, X. X. Li, W. H. Fang, G. Y. Yang, *J. Am. Chem. Soc.* **2010**, *132*, 15102–15103; h) B. Li, J. W. Zhao, S. T. Zheng, G. Y. Yang, *Inorg. Chem.* **2009**, *48*, 8294–8303.

[3] a) F. Hussain, R. W. Gable, M. Speldrich, P. Kögerler, C. Boskovic, *Chem. Commun.* **2009**, 328–330; b) C. Ritchie, C. E. Miller, C. Boskovic, *Dalton Trans.* **2011**, *40*, 12037–12039; c) L. Ni, F. Hussain, B. Spingler, S. Weyeneth, G. R. Patzke, *Inorg. Chem.* **2011**, *50*, 4944–4955; d) C. Ritchie, V. Baslon, E. G. Moore, C. Reber, C. Boskovic, *Inorg. Chem.* **2012**, *51*, 1142–1151; e) M. Zimmermann, N. Belai, R. J. Butcher, M. T. Pope, E. V. Chubarova, M. H. Dickman, U. Kortz, *Inorg. Chem.* **2007**, *46*, 1737–1740; f) S. Cardona-Serra, J. M. Clemente-Juan, E. Coronado, A. Gaita-Ariño, A. Camón, M. Evangelisti, F. Luis, M. J. Martínez-Pérez, J. Sesé, *J. Am. Chem. Soc.* **2012**, *134*, 14982–14990; g) J. A. Fernández, X. López, C. Bo, C. de Graaf, E. J. Baerends, J. M. Poblet, *J. Am. Chem. Soc.* **2007**, *129*, 12244–12253; h) K.-C. Kim, M. T. Pope, G. J. Gama, M. H. Dickman, *J. Am. Chem. Soc.* **1999**, *121*, 11164–11170.

[4] R. D. Peacock, T. J. R. Weakley, *J. Chem. Soc. A* **1971**, 1836–1839.

[5] a) K. Wassermann, M. H. Dickman, M. T. Pope, *Angew. Chem.* **1997**, *109*, 1513–1516; *Angew. Chem. Int. Ed. Engl.* **1997**, *36*, 1445–1448; b) R. C. Howell, F. G. Perez, S. Jain, W. D. Horrocks, Jr., A. L. Rheingold, L. C. Francesconi, *Angew. Chem.* **2001**, *113*, 4155–4158; *Angew. Chem. Int. Ed.* **2001**, *40*, 4031–4034; c) B. S. Bassil, M. H. Dickman, I. Römer, B. von der Kammer, U. Kortz, *Angew. Chem.* **2007**, *119*, 6305–6308; *Angew. Chem. Int. Ed.* **2007**, *46*, 6192–6195.

[6] F. Hussain, F. Conrad, G. R. Patzke, *Angew. Chem.* **2009**, *121*, 9252–9255; *Angew. Chem. Int. Ed.* **2009**, *48*, 9088–9091.

[7] S. Reinoso, M. Giménez-Marqués, J. R. Galán-Mascarós, P. Vitoria, J. M. Gutiérrez-Zorrilla, *Angew. Chem.* **2010**, *122*, 8562–8566; *Angew. Chem. Int. Ed.* **2010**, *49*, 8384–8388.

[8] F. Hussain, G. R. Patzke, *CrystEngComm* **2011**, *13*, 530–536.

[9] G. Xue, B. Liu, H. Hu, J. Yang, J. Wang, F. Fu, *J. Mol. Struct.* **2004**, *690*, 95–103.

[10] A. Merca, A. Müller, J. van Slageren, M. Läge, B. Krebs, *J. Cluster Sci.* **2007**, *18*, 711–719.

[11] J. Cao, S. Liu, R. Cao, L. Xie, Y. Ren, C. Gao, L. Xu, *Dalton Trans.* **2008**, 115–120.

[12] a) W. Chen, Y. Li, Y. Wang, E. Wang, *Eur. J. Inorg. Chem.* **2007**, 2216–2220; b) W. L. Chen, Y. G. Li, Y. H. Wang, E. B. Wang, Z. M. Zhang, *Dalton Trans.* **2008**, 865–867; c) Z. Zhang, Y. Li, W. Chen, E. Wang, X. Wang, *Inorg. Chem. Commun.* **2008**, *11*, 879–882; d) Z. M. Zhang, Y. G. Li, S. Yao, E. B. Wang, *Dalton Trans.* **2011**, *40*, 6475–6479; e) H. H. Wu, S. Yao, Z. M. Zhang, Y. G. Li, Y. Song, Z. J. Liu, X. B. Han, E. B. Wang, *Dalton Trans.* **2013**, *42*, 342–346.

[13] H. Pang, C. Zhang, D. Shi, Y. Chen, *Cryst. Growth Des.* **2008**, *8*, 4476–4480.

[14] a) S. Reinoso, J. R. n. Galán-Mascarós, *Inorg. Chem.* **2010**, *49*, 377–379; b) S. Reinoso, J. R. Galán-Mascarós, L. Lezama, *Inorg. Chem.* **2011**, *50*, 9587–9593.

[15] a) B. Nohra, P. Mialane, A. Dolbecq, E. Riviere, J. Marrot, F. Secheresse, *Chem. Commun.* **2009**, 2703–2705; b) J. D. Compain, P. Mialane, A. Dolbecq, I. M. Mbomekallé, J. Marrot, F. Sécheresse, C. Duboc, E. Rivie're, *Inorg. Chem.* **2010**, *49*, 2851–2858.

[16] a) S. W. Zhang, J. W. Zhao, P. T. Ma, J. Y. Niu, J. P. Wang, *Chem. Asian J.* **2012**, *7*, 966–974; b) S. W. Zhang, Y. Wang, J. W. Zhao, P. T. Ma, J. P. Wang, J. Y. Niu, *Dalton Trans.* **2012**, *41*, 3764–3772; c) J. W. Zhao, J. Luo, L. J. Chen, J. Yuan, H. Y. Li, P. T. Ma, J. P. Wang, J. Y. Niu, *CrystEngComm* **2012**, *14*, 7981–7993.

[17] a) H.-Y. Zhao, J.-W. Zhao, B.-F. Yang, H. He, G.-Y. Yang, *CrystEngComm* **2013**, *15*, 5209–5213; b) H.-Y. Zhao, J.-W. Zhao, B.-F. Yang, H. He, G.-Y. Yang, *CrystEngComm* **2013**, *15*, 8186–8194.

[18] a) Y. H. Liu, G. L. Guo, J. P. Wang, *J. Coord. Chem.* **2008**, *61*, 2428–2436; b) J. Wang, W. Wang, Q. Yan, J. Niu, *J. Rare Earth* **2008**, *26*, 638–642; c) J. P. Wang, Q. X. Yan, X. D. Du, J. Y. Niu, *J. Cluster Sci.* **2008**, *19*, 491–498; d) J. P. Wang, Q. X. Yan, X. D. Du, J. Y. Niu, *Chin. J. Chem.* **2008**, *26*, 1239–1243; e) B. Li, J. W. Zhao, S. T. Zheng, G. Y. Yang, *J. Cluster Sci.* **2009**, *20*, 503–513; f) D. Du, J. Qin, S. Li, Y. Lan, X. Wang, Z. Su, *Aust. J. Chem.* **2010**, *63*, 1389–1395; g) L. Chen, D. Shi, Y. Wang, H. Cheng, Z. Geng, J. Zhao, P. Ma, J. Niu, *J. Coord. Chem.* **2011**, *64*, 400–412; h) J. Niu, S. Zhang, H. Chen, J. Zhao, P. Ma, J. Wang, *Cryst. Growth Des.* **2011**, *11*, 3769–3777; i) D. Shi, L. Chen, J. Zhao, Y. Wang, P. Ma, J. Niu, *Inorg. Chem. Commun.* **2011**, *14*, 324–329; j) J. Luo, C. Leng, L. Chen, J. Yuan, H. Li, J. Zhao, *Synth. Met.* **2012**, *162*, 1558–1565; k) S. S. Shang, J. W. Zhao, L. J. Chen, Y. Y. Li, J. L. Zhang, Y. Z. Li, J. Y. Niu, *J. Solid State Chem.* **2012**, *196*, 29–39; l) D. Y. Shi, J. W. Zhao, L. J. Chen, P. T. Ma, J. P. Wang, J. Y. Niu, *CrystEngComm* **2012**, *14*, 3108–3119; m) D. D. Zhang, S. W. Zhang, P. T. Ma, J. P. Wang, J. Y. Niu, *Inorg. Chem. Commun.* **2012**, *20*, 191–195; n) S. W. Zhang, J. W. Zhao, P. T. Ma, H. N. Chen, J. Y. Niu, J. P. Wang, *Cryst. Growth Des.* **2012**, *12*, 1263–1272; o) J. W. Zhao, D. Y. Shi, L. J. Chen, Y. Z. Li, P. T. Ma, J. P. Wang, J. Y. Niu, *Dalton Trans.* **2012**, *41*, 10740–10751; p) J. Luo, J. W. Zhao, J. Yuan, Y. Z. Li, L. J. Chen, P. T. Ma, J. P. Wang, J. Y. Niu, *Inorg. Chem. Commun.* **2013**, *27*, 13–17.

[19] a) X. K. Fang, P. Kogerler, *Chem. Commun.* **2008**, 3396–3398; b) X. K. Fang, P. Kögerler, *Angew. Chem.* **2008**, *120*, 8243–8246; *Angew. Chem. Int. Ed.* **2008**, *47*, 8123–8126.

[20] a) S. Yao, Z. M. Zhang, Y. G. Li, Y. Lu, E. B. Wang, Z. M. Su, *Cryst. Growth Des.* **2010**, *10*, 135–139; b) Y. W. Li, Y. G. Li, Y. H. Wang, X. J. Feng, Y. Lu, E. B. Wang, *Inorg. Chem.* **2009**, *48*, 6452–6458.

[21] A. H. Ismail, B. S. Bassil, G. H. Yassin, B. Keita, U. Kortz, *Chem. Eur. J.* **2012**, *18*, 6163–6166.

[22] C. Preyssler, *Bull. Soc. Chim. Fr.* **1970**, 30–36.

[23] M. H. Alizadeh, S. P. Harmalker, Y. Jeannin, J. Martin-Frere, M. T. Pope, *J. Am. Chem. Soc.* **1985**, *107*, 2662–2669.

[24] F. F. Bamoharram, M. Roshani, M. H. Alizadeh, H. Razavi, M. Moghayadi, *J. Braz. Chem. Soc.* **2006**, *17*, 505–509.

[25] a) S. Q. Liu, D. G. Kurthe, H. Möhwald, D. Volkmer, *Adv. Mater.* **2002**, *14*, 225–228; b) T. R. Zhang, R. Lu, X. L. Liu, Y. Y. Zhao, T. J. Li, J. N. Yao, *J. Solid State Chem.* **2003**, *172*, 458–463; c) S. Q. Liu, H. Möhwald, D. Volkmer, D. G. Kurth, *Langmuir* **2006**, *22*, 1949–1951.

[26] M. Rahimizadeh, T. Bazazan, A. Shiri, M. Bakavoli, H. Hassani, *Chin. Chem. Lett.* **2011**, *22*, 435–438.

[27] a) C. Qin, X. Z. Song, S. Q. Su, S. Dang, J. Feng, S. Y. Song, Z. M. Hao, H. J. Zhang, *Dalton Trans.* **2012**, *41*, 2399–2407; b) L. Huang, L. Cheng, S. S. Wang, W. H. Fang, G. Y. Yang, *Eur. J. Inorg. Chem.* **2013**, 1639–1643; c) Y. Lu, Y. Li, E. Wang, X. Xu, Y. Ma, *Inorg. Chim. Acta* **2007**, *360*, 2063–2070; d) C. Y. Yang, L. C. Zhang, Z. J. Wang, L. Wang, X. H. Li, Z. M. Zhu, *J. Solid State Chem.* **2012**, *194*, 270–276; e) X. Wang, J. Li, A. Tian, H. Lin, G. Liu, H. Hu, *Inorg. Chem. Commun.* **2011**, *14*, 103–106.

[28] S. T. Zheng, D. Q. Yuan, H. P. Jia, J. Zhang, G. Y. Yang, *Chem. Commun.* **2007**, 1858–1860.

[29] S. T. Zheng, D. Q. Yuan, J. Zhang, G. Y. Yang, *Inorg. Chem.* **2007**, *46*, 4569–4574.

[30] J. W. Zhao, H. P. Jia, J. Zhang, S. T. Zheng, G. Y. Yang, *Chem. Eur. J.* **2007**, *13*, 10030–10045.

[31] J. W. Zhao, J. Zhang, S. T. Zheng, G. Y. Yang, *Chem. Commun.* **2008**, 570–572.
[32] X. X. Li, S. T. Zheng, J. Zhang, W. H. Fang, G. Y. Yang, J. M. Clemente-Juan, *Chem. Eur. J.* **2011**, *17*, 13032–13043.
[33] a) L. Huang, J. Zhang, L. Cheng, G. Y. Yang, *Chem. Commun.* **2012**, *48*, 9658–9660; b) Y. H. Liu, S. Z. Liu, *Acta Crystallogr. Sect. E* **2007**, *63*, m312–m313.
[34] I. D. Brown, D. Altermatt, *Acta Crystallogr. Sect. B* **1985**, *41*, 244–247.
[35] H. An, H. Zhang, Z. Chen, Y. Li, X. Liu, H. Chen, *Dalton Trans.* **2012**, *41*, 8390–8400.
[36] J. Niu, K. Wang, H. Chen, J. Zhao, P. Ma, J. Wang, M. Li, Y. Bai, D. Dang, *Cryst. Growth Des.* **2009**, *9*, 4362–4372.
[37] L. Armelao, S. Quici, F. Barigelletti, G. Accorsi, G. Bottaro, M. Cavazzini, E. Tondello, *Coord. Chem. Rev.* **2010**, *254*, 487–505.
[38] G. J. Sopasis, M. Orfanoudaki, P. Zarmpas, A. Philippidis, M. Siczek, T. Lis, J. R. O'Brien, C. J. Milios, *Inorg. Chem.* **2012**, *51*, 1170–1179.
[39] a) S. L. Cai, S. R. Zheng, Z. Z. Wen, J. Fan, W. G. Zhang, *Cryst. Growth Des.* **2012**, *12*, 5737–5745; b) R. W. Ricci, K. B. Kilichowski, *J Phys. Chem.* **1974**, *78*, 1953–1956.
[40] W. T. Chen, S. Fukuzumi, *Inorg. Chem.* **2009**, *48*, 3800–3807.
[41] a) T. Ito, H. Yashiro, T. Yamase, *Langmuir* **2006**, *22*, 2806–2810; b) T. Yamase, *Chem. Rev.* **1998**, *98*, 307–325.
[42] A. P. Ginsberg, *Inorganic Syntheses*, *Vol. 27*, Wiley, New York, **1990**, pp. 105–106.
[43] a) G. M. Sheldrick, *SHELXS97*, *Program for Crystal Structure Solution*, University of Göttingen, Göttingen, Germany, **1997**; b) G. M. Sheldrick, *SHELXL97*, *Program for Crystal Structure Refinement*, University of Göttingen, Göttingen, Germany, **1997**.

Received: September 26, 2013
Revised: November 4, 2013
Published online: December 2, 2013

